Geophysical Research Letters

RESEARCH LETTER
10.1029/2020GL087215

Special Section:
New Understanding of the Arabian Sea Circulation

Equatorial Circulation in the Western Indian Ocean During Onset of the 2018 Summer Monsoon and Links to the Bay of Bengal

Robert E. Todd[1]

[1]Woods Hole Oceanographic Institution, Woods Hole, MA, USA

Key Points:
- Autonomous and ship-based observations capture circulation changes in the western equatorial Indian Ocean during monsoon transition
- A first-mode baroclinic Kelvin wave passed through the region, but observed vertical structure of currents was consistent with higher modes
- A strong equatorial undercurrent in March 2018 carried salty waters from the Arabian Sea that later reached the central Bay of Bengal

Correspondence to:
R. E. Todd,
rtodd@whoi.edu

Citation:
Todd, R. E. (2020). Equatorial circulation in the western Indian Ocean during onset of the 2018 summer monsoon and links to the Bay of Bengal. *Geophysical Research Letters*, *47*, e2020GL087215. https://doi.org/10.1029/2020GL087215

Received 22 JAN 2020
Accepted 26 FEB 2020
Accepted article online 29 FEB 2020

Abstract Cross-equator transects occupied by an underwater glider and a research vessel in the western Indian Ocean captured the evolution of equatorial circulation during onset of the boreal summer monsoon in 2018. At the end of the winter monsoon in March, surface currents were westward, while the equatorial undercurrent carried salty Arabian Sea High-Salinity Water eastward. As winds transitioned from westward to eastward during April, an eastward near-surface Wyrtki Jet developed, while the equatorial undercurrent weakened, vanishing by May. A first-mode baroclinic Kelvin wave propagated through the survey region after westward winds relaxed. However, the vertical structure of the evolving circulation was inconsistent with the first baroclinic mode, suggesting the influence of higher modes in setting observed vertical structure. The strong equatorial undercurrent at the end of the winter monsoon allowed high-salinity waters from the western equatorial Indian Ocean to reach the southern Bay of Bengal in summer 2018.

Plain Language Summary Circulation throughout the Indian Ocean is strongly influenced by the twice-per-year reversal of the monsoon winds over the basin. New observations collected using both an autonomous underwater glider and a research vessel in 2018 captured the reversal of layered currents in the upper ocean as the northeast (winter) monsoon gave way to the southwest (summer) monsoon. From March to May, near-surface currents switched form westward to eastward, while the eastward equatorial undercurrent weakened and vanished. Equatorial planetary waves play a key role in propagating signals, such as those associated with changing monsoon winds, through the equatorial oceans. An eastward propagating Kelvin wave moving at a speed consistent with the first baroclinic mode was detected by satellite, but the observed vertical structure of the changing currents during the monsoon transition was inconsistent with the first baroclinic mode. Higher-mode waves are suspected to play a role in the evolution of equatorial currents during the monsoon transition. Relatively strong subsurface flow at the end of the winter monsoon carried salty waters originating in the Arabian Sea eastward, leading to a salty subsurface feature in the Bay of Bengal in summer 2018.

1. Introduction

In the equatorial oceans, the basic zonal circulation consists of surface flow in the same direction as the equatorial winds that in turn sets up a baroclinic zonal pressure gradient that drives return flow opposing the wind along the thermocline (McPhaden, 1986; Philander, 1973). In the Pacific and Atlantic, westward trade winds dominate, and the resulting westward surface flow and eastward equatorial undercurrents (EUCs) are nearly always found. However, oceanic circulation throughout the Indian Ocean is largely controlled by the Asian monsoon cycle (Schott & McCreary, 2001). During April–June and October–November, winds over the equatorial Indian Ocean have an eastward component (Schott & McCreary, 2001), contrary to the usual situation in the Pacific and Atlantic. This variability in zonal wind stress leads to semiannual variability in the upper ocean currents, modulated in part by propagation of equatorial waves (e.g., Iskander & McPhaden, 2011; Nagura & McPhaden, 2010; Yuan & Han, 2006). In particular, the EUC is a transient feature in the Indian Ocean, and strong eastward Wyrtki Jets develop near the surface during intermonsoon periods (Nagura & McPhaden, 2010; Wyrtki, 1973).

The transient nature of the EUC in the Indian Ocean has been known since the first International Indian Ocean Experiment in 1962–1965. Measurements in June–September 1962 showed no evidence of an

©2020. American Geophysical Union. All Rights Reserved.

eastward EUC in the Indian Ocean (Knauss & Taft, 1963). Using observations collected in February–May 1963, Knauss and Taft (1964) first documented the Indian Ocean EUC. Swallow (1964) found a stronger EUC during the same time period of the following year. In the ensuing decades, a variety of ship-based (e.g., Knox, 1974; Leetmaa & Stommel, 1980) and moored observations (e.g., Chen et al., 2015; Iskander et al., 2009; Reppin et al., 1999) have made clear that the EUC in the Indian Ocean consistently appears in boreal winter and spring and reappears during late summer and early fall of some years (Chen et al., 2015; Schott & McCreary, 2001). Analyses of available in situ and remotely sensed time series combined with numerical simulations have shown that much of this variability is tied to wind-driven equatorial Kelvin waves and Rossby waves reflected from the eastern boundary (e.g., Chen et al., 2015; Iskander et al., 2009).

Alternating monsoon-driven currents are key to maintaining the salinity balance of the northern Indian Ocean (Lee et al., 2016) as they export saline waters from the evaporative Arabian Sea and remove freshwater from the Bay of Bengal, which receives large riverine input (e.g., Rao & Sivakumar, 2003). Sanchez-Franks et al. (2019) recently demonstrated that interannual variability in the strength of the EUC acts to control salinity within a subsurface high-salinity core (HSC) in the central Bay of Bengal. In years when the EUC is strong during the winter monsoon, Arabian Sea High-Salinity Water (ASHSW; Kumar & Prasad, 1999; Shenoi et al., 1993; Rochford, 1964) is advected from the western equatorial Indian Ocean quickly enough to be entrained into the Southwest Monsoon Current, which then brings the waters into the Bay of Bengal, feeding a particularly salty HSC. In years with a weak EUC during the winter monsoon, high-salinity water from the western equatorial Indian Ocean fails to reach the Bay of Bengal.

For roughly two decades prior to 2018, research vessel access to the northwestern Indian Ocean and Arabian Sea was restricted due to the threat of piracy in the region. As a result, detailed, high-resolution surveys of the equatorial circulation have been limited. Observations from moored acoustic Doppler current profilers (ADCPs) along the equator as part of the Research Moored Array for African-Asian-Australian Monsoon Analysis and Prediction (RAMA; McPhaden et al., 2009) provide time series of currents and water properties directly on the equator (e.g., Chen et al., 2015; Iskander et al., 2009) but do not resolve the meridional extent of equatorial flows and do not yet extend west of 65°E. Surface drifters from the Global Drifter Program have provided important insights about near-surface circulation, and subsurface profiles from the Argo program (Riser et al., 2016) have provided important broad-scale measurements. In 2016–2018, the Office of Naval Research's "Northern Arabian Sea Circulation—autonomous research (NASCar)" Defense Research Initiative (Centurioni et al., 2017) deployed a variety autonomous sampling platforms to fill the observational gap in the northwestern Indian Ocean. Additionally, the Global Ocean Ship-Based Hydrographic Investigations Program (GO-SHIP; Sloyan et al., 2019) program reoccupied a hydrographic line through the Arabian Sea in 2018.

Here we present a novel set of observation from NASCar and GO-SHIP (section 2) that provide a detailed view of the circulation in the western equatorial Indian Ocean during the spring monsoon transition of 2018 (section 3.1). We further demonstrate that a strong EUC in the western Indian Ocean during spring 2018 fed a strong HSC in the Bay of Bengal in summer 2018 (section 3.2). Section 4 then summarizes the results and implications.

2. Observations and Reanalysis

2.1. Spray Glider Observations

Spray autonomous underwater gliders (Sherman et al., 2001; Rudnick et al., 2016) sampled the equatorial Indian Ocean during March–May of 2017 and 2018 as part of NASCar. Observations from 2017 were presented in Centurioni et al. (2017), and our focus here is on more comprehensive observations collected in 2018. On 1 March 2018, a single Spray glider was deployed near Denis Island, Seychelles, from Seychelles Coast Guard patrol ship *Constant*. The glider was piloted northeastward to 1°S, 57°40′E and then repeatedly occupied a cross-equator transect along 57°40′E (Figure 1a). The glider mission was purposefully timed to capture the transition from the boreal winter (northeast) monsoon to the summer (southwest) monsoon at the equator. The glider completed four surveys across the equator between 16 March and 17 May; the first two extended as far north as 1°30′N, while the latter two were limited in northward extent to 0°10′N by constraints on mission length (Figure 1c, orange). The glider was piloted back to the eastern edge of the Mascarene Plateau, where it was recovered using Seychelles Coast Guard patrol ship *Etoile* on 26 June (Figure 1a).

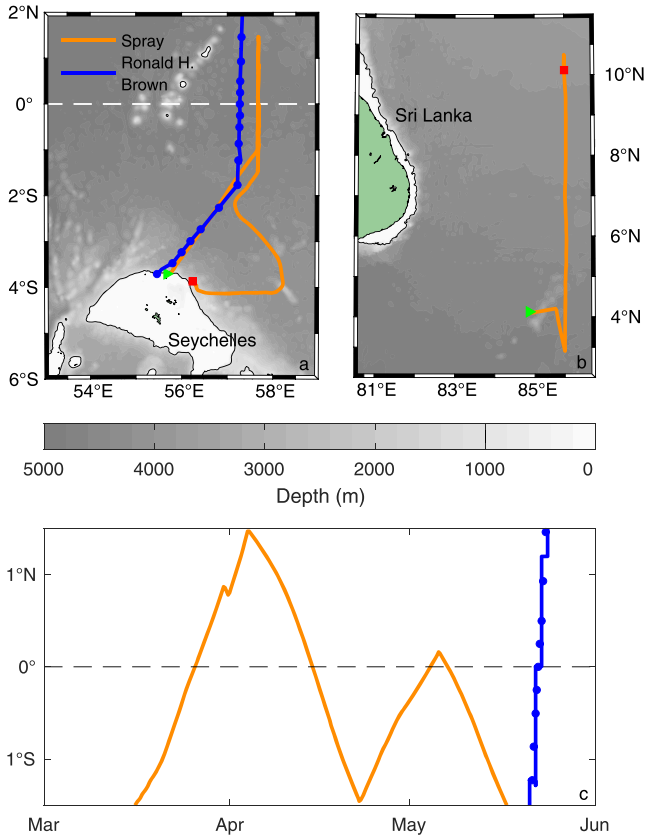

Figure 1. (a) Map of the equatorial Indian Ocean near the Seychelles with locations of glider- (orange) and ship-based (blue) observations during 2018. Dots along the track of the *Ronald H. Brown* indicate locations of hydrographic stations. The 1,000-m isobath is drawn in black. (b) Map of the southwestern Bay of Bengal with locations of glider observations during 2018 (orange). (c) Time-latitude distribution of sampling within 1.5° of the equator in 2018.

The glider carried a pumped Sea-Bird 41CP conductivity-temperature-depth (CTD) instrument, a 1-MHz Nortek AD2CP Doppler current profiler, and a Seapoint chlorophyll fluorometer that each measured during the ascending phase of each dive. Profiles of temperature, salinity, density, and chlorophyll fluorescence were averaged into 10-m vertical bins following manual quality control of full-resolution (0.125 Hz, or about 0.8 m in the vertical) data. Profiles of absolute horizontal velocity were estimated from AD2CP-derived shear and measured depth-average currents (Rudnick et al., 2018) following Todd et al. (2017), including corrections for biofouling and with updates to quality control thresholds as described by Todd et al. (2018). As an estimate of the root-mean-square accuracy of the velocity profiles, we follow Todd et al. (2017) and assume that velocity variance should generally decrease with increasing depth; any increase in variance below a midprofile minimum is taken to be due to errors in the velocity solution. The resulting upper bound on root-mean-square error in velocity profiles is 0.06 m s^{-1} for this glider mission, which is in addition to the O(0.01) m s^{-1} error inherent in the depth-average velocities (Rudnick et al., 2018) that profiles are constrained to match. Here we focus on measurements of eastward velocity, salinity, temperature, and density from the four cross-equator transects occupied by the glider in 2018 (Figures 2a–2h).

In addition to the NASCar glider observations, we make use of hydrographic measurements from a similarly equipped Spray glider that surveyed in the southern Bay of Bengal as part of the Office of Naval Research-sponsored "Oceanic Control of Monsoon Intra-seasonal Oscillations in the Tropical Indian Ocean and the Bay of Bengal (MISO-BOB)" Defense Research Initiative. That glider was deployed from R/V *Thomas G. Thompson* on 29 May 2018, then primarily surveyed northward along 85°45′E from 3°8′N to 10°30′N before being recovered by R/V *Thompson* on 9 July 2018 (Figure 1b).

2.2. GO-SHIP Observations

As part of GO-SHIP, NOAA ship *Ronald H. Brown* occupied the I07N hydrographic line between Durban, South Africa, and Goa, India, with a port call in Victoria, Seychelles, during April–June 2018. The ship

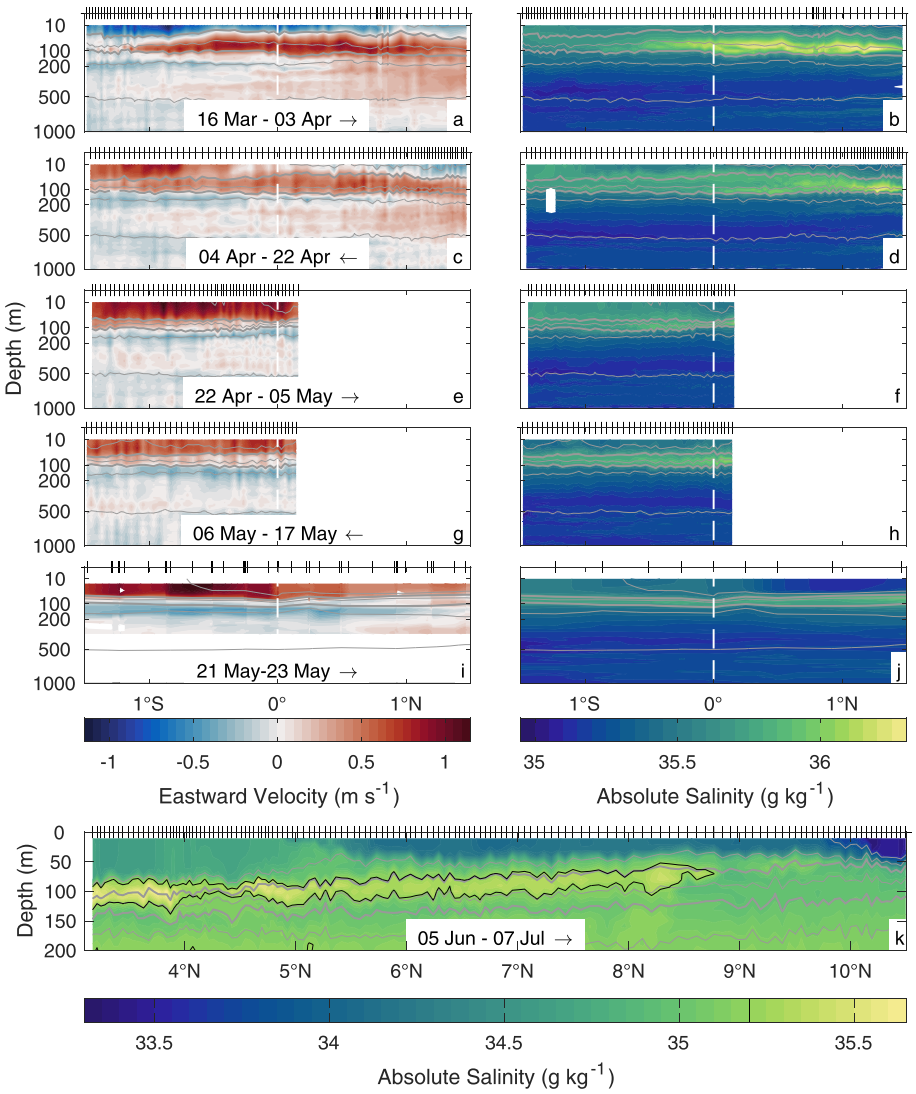

Figure 2. (a–j) Cross-equator transects of (left) zonal velocity and (right) salinity in the upper 1,000 m during March–May 2018 that were occupied by Spray gliders (a–h) and NOAA ship *Ronald H. Brown* (i, j) in the western Indian Ocean. Gray contours are isopycnals with a contour interval of 1.0 kg m^{-3} and the 23.0 and 25.0 kg m^{-3} isopycnals in bold. Tick marks on the upper axes denote locations of individual profiles. Dates of each transect and direction of platform motion are indicated in the velocity panels. The white dashed line indicates the equator in each panel. Note the stretched vertical coordinate. (k) Salinity measured by a Spray glider along 85°45′E in the Bay of Bengal with plot features as above except for changes in depth range and scale, salinity range, and addition of the 35.2 g kg^{-1} isohaline in black to highlight the HSC in the Bay of Bengal.

sampled northbound across the equator near 57°15′E between 1°46′S and 2°N during 21–23 May, just after the glider completed its last southbound transect (Figure 1b, blue). Here we use CTD profiles collected with the vessel's Sea-Bird 9plus at 11 stations spanning the equator (Figure 1a, blue dots) and upper ocean velocity profiles from the vessel's hull-mounted 75-kHz RDI Ocean Surveyor operating in broadband mode. CTD profiles are binned from 1-db resolution to 10-m vertical resolution to match glider observations, and velocity profiles are averaged to hourly resolution (Figures 2i and 2j).

2.3. Sea Surface Products

Estimates of winds at 10-m height were obtained from the European Centre for Medium-Range Weather Forecasts (ECMWF) ERA-Interim reanalysis product (Dee et al., 2011) at a resolution of 0.75° × 0.75°. Zonal winds within 1.5° latitude of the equator were averaged meridionally and low-pass filtered with a 20-day cut-off period (Figure 3a). Estimates of absolute dynamic topography (ADT) on a 0.25° × 0.25° grid were obtained from the Copernicus Marine Environment Monitoring Service (CMEMS). To highlight signals associated

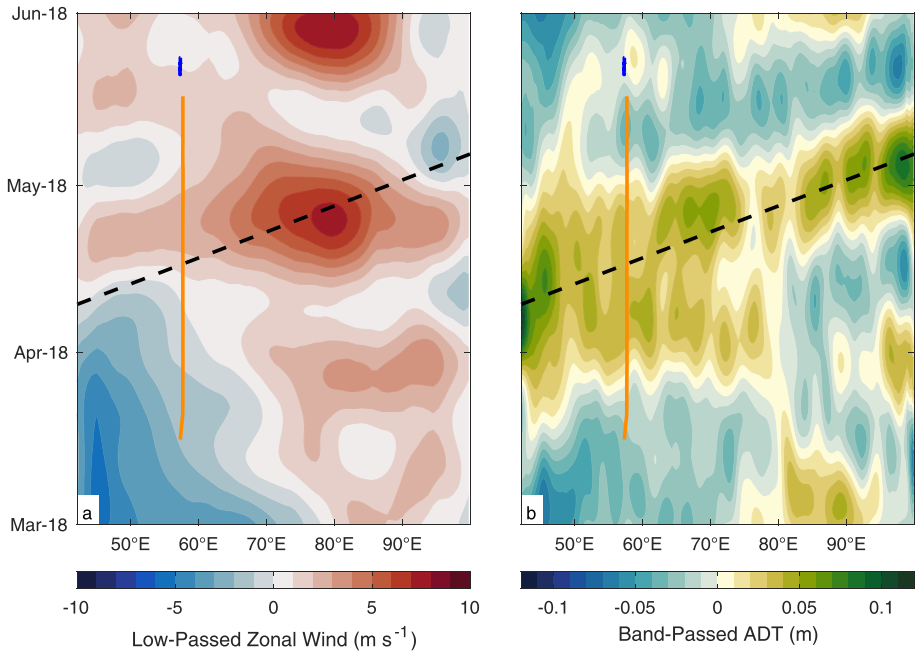

Figure 3. Time-longitude plots of (a) low-pass filtered zonal winds and (b) band-passed ADT averaged within 1.5° latitude of the equator across the Indian Ocean. In both panels, the orange line is the glider's trajectory while it was within 1.5° latitude of the equator, the blue line is the ship's trajectory within 1.5° latitude of the equator, and the dashed black line represents propagation of a first-mode baroclinic Kelvin wave starting at the western boundary on 10 April.

with equatorial waves, ADT within 1.5° latitude of the equator was averaged meridionally and band-pass filtered with 20- and 180-day cutoff periods (Figure 3b).

2.4. Equatorial Sampling Relative to Monsoon Transition

The transition from winter to summer monsoon in the western equatorial Indian Ocean is marked by relaxation of westward zonal winds, particularly along the western boundary near 42°54′E. In 2018, zonal winds between the African coast and the glider- and ship-based observations near 57°30′E first changed sign around 10 April and were persistently eastward at the longitude of the glider and ship-based observations for the remainder of the observation period (Figure 3a). The first northbound glider transect (Figures 2a and 2b) and the northern half of the first southbound transect (Figures 2c and 2d) were completed before zonal winds changed sign. Subsequent transects were occupied after the relaxation of westward winds.

3. Results and Discussion

3.1. Equatorial Circulation During Monsoon Transition

To characterize the temporal evolution of circulation in the western equatorial Indian Ocean during onset of the 2018 summer monsoon, we consider both distinct cross-equator transects of upper ocean properties with no horizontal averaging (Figure 2) and profiles averaged within 0°10′ latitude of the equator and 1°N from each transect (Figure 4). The full transects capture the meridional structure of the circulation. Averaged profiles highlight the changing vertical structure of the circulation at intervals of 2–3 weeks.

3.1.1. Near Surface

Near-surface currents switched from westward to eastward over a period of a few weeks during the monsoon transition. Prior to monsoon onset, near-surface currents were strongly westward with magnitudes as large as 1.1 m s^{-1} and extended from the surface to near the 23.0 kg m^{-3} isopycnal, which was typically found at depths of 20–40 m (Figures 2a, 2c, and 4a). Near-surface currents relaxed in early April (Figure 2c), roughly coinciding with the change in direction of zonal winds near the equator (Figure 3a). Near-surface currents then became strongly eastward during late April and May (Figures 2e, 2g, 2i, and 4a) as the Wyrtki Jet developed. Eastward currents near the surface exceeded 1.2 m s^{-1} south of the equator in both glider observations (Figure 2e) and shipboard ADCP measurements (Figure 2i). From late April through May, strong eastward

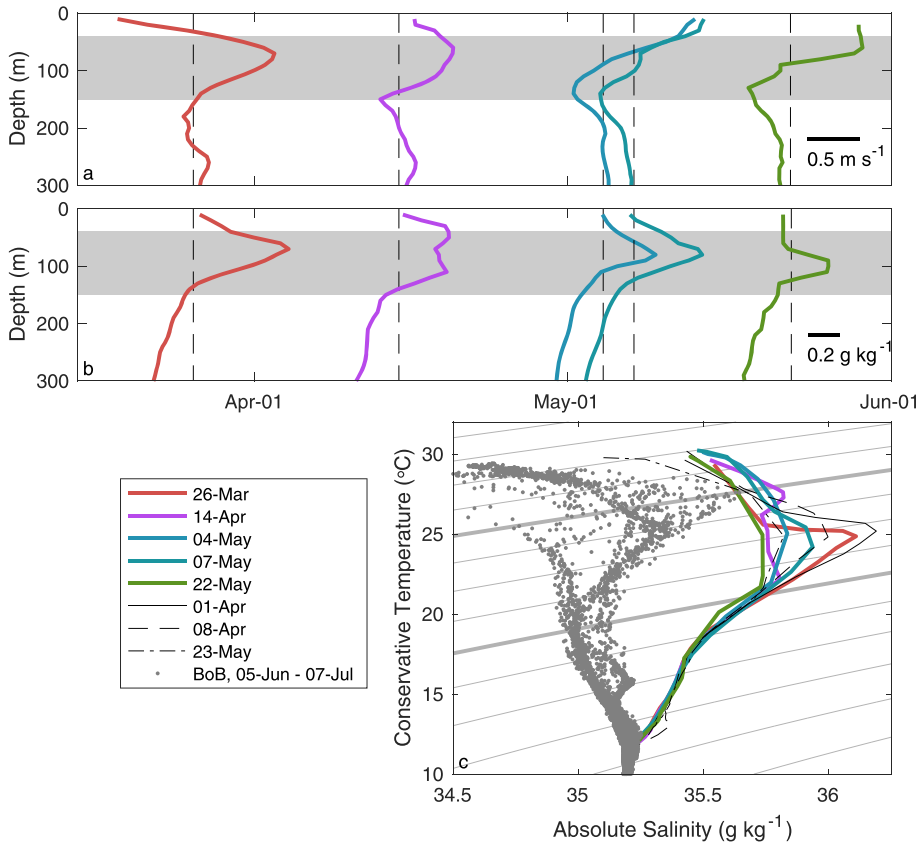

Figure 4. Temporal evolution along the equator during March–May of 2018. (a) Zonal velocity profiles averaged between 0°10′S and 0°10′N for each transect with dashed lines at the time of each equator crossing denoting zero velocity for each profile; a scale bar is in the lower right. Gray shading from 40 to 150 m denotes the depth range of the EUC when present. (b) Salinity profiles averaged as in (a) with dashed lines denoting a salinity of 35.5 g kg^{-1} for each profile and a scale bar in the lower right. (c) Temperature-salinity curves corresponding to each equator crossing (color) as well as for the three crossings of 1°N (black lines) and along 85°45′E in the Bay of Bengal (BoB) during June–July 2018 (gray dots). Gray contours are isopycnals with a contour interval of 0.5 kg m^{-3} and the 23.0 and 25.0 kg m^{-3} isopycnals in bold.

flow was generally shallower than the 23.0 kg m^{-3} isopycnal (Figures 2e, 2g, and 2i), as were strong westward flows before. However, the depth of that isopycnal was notably deeper after onset of the monsoon, typically around 50–70 m (Figure 2).

Water properties above the 23.0 kg m^{-3} isopycnal changed little along the equator (Figures 4b and 4c) and farther south (Figure 2) during March–May. However, near 1°N, near-surface waters freshened by about 0.3 g kg^{-1} (Figure 4c, black curves) between the glider sampling in late March to early April (Figures 2b and 2d) and the ship-based sampling in the latter part of May (Figure 2j). We note that the magnitude of this salinity change at 1°N is much larger than O(0.01) g kg^{-1} difference between deep salinities measured by the glider and by the ship (Figure 4c) and so does not result from calibration differences between instruments. It is plausible that these eastward flowing (Figure 2i), relatively fresh waters (salinity less than 35.4 g kg^{-1}) originated in the Bay of Bengal, were advected into the central Arabian Sea by the Northeast Monsoon Current (Lee et al., 2016; Schott & McCreary, 2001), and subsequently entrained into the equatorial circulation.

3.1.2. Subsurface

At the end of the northeast monsoon, the EUC appeared as a well-developed, subsurface eastward current below the westward surface flow and was generally bounded by the 23.0 and 25.0 kg m^{-3} isopycnals (Figure 2a). The EUC was located at depths of 40–150 m (gray shading in Figures 4a and 4b) with a maximum speed of 0.95 m s^{-1} at 70 m near 0.5°N (Figure 2a) and a peak speed of 0.77 m s^{-1} on the equator (Figure 4a). Eastward volume transport shallower than 180 m and between 1.5°S and 1.5°N during this time was 15.7 Sv, in good agreement with the maximum transport of 17 Sv reported by Reppin et al. (1999) for a similar time of year at 80°30′E. During April and May, the eastward flow of the EUC weakened and then

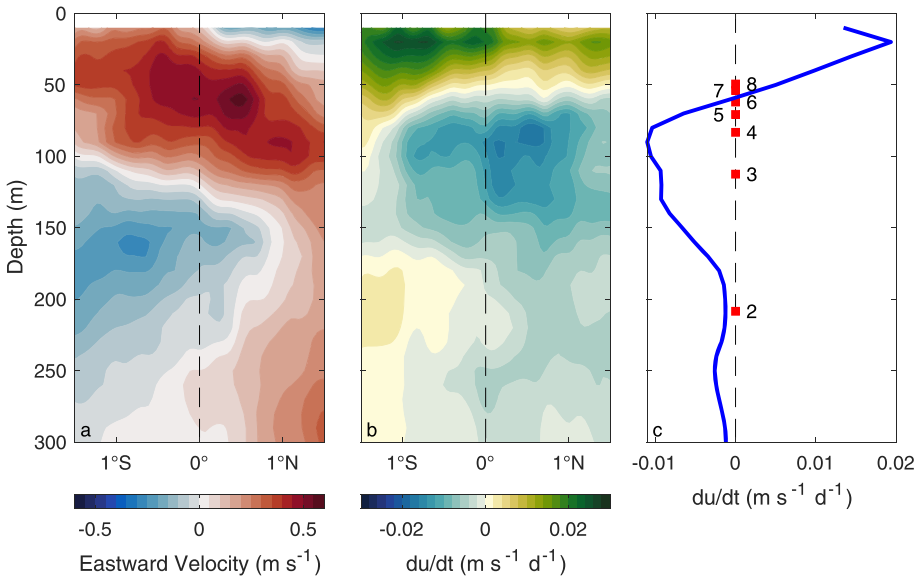

Figure 5. Least squares fits of the (a) mean and (b) rate of change of zonal velocity between 1.5°S and 1.5°N during March–May 2018; the dashed line denotes the equator. (c) Meridionally averaged rate of change of zonal velocity (blue) with shallowest zero crossings of the second through eighth baroclinic modes denoted by the numbered red squares.

became indistinct from the developing eastward flow in the surface layer (Figures 2c, 2e, 2g, 2i, and 4a). By May, flow below 100 m had reversed direction (Figures 2e, 2g, 2i, and 4a).

Eastward flow at depths of 200–500 m extended from 1°S to the northern limit of the observations during March–April (Figures 2a and 2c), merging with the shallower EUC flow north of about 1°N. This eastward flow is consistent with the Equatorial Intermediate Current (EIC) described by Huang et al. (2018) using moored observation in the eastern Indian Ocean. Like shallower flows, the EIC has been shown to have distinct semiannual variability (Huang et al., 2018; Luyten & Roemmich, 1982); eastward flow during March–April at 57°40′E is consistent with the phasing suggested by a reanalysis-based climatology (Huang et al., 2018).

3.1.3. Role of Equatorial Waves

To examine whether the changes in circulation discussed above result from equatorial wave propagation, we compute phase speeds and vertical structures for baroclinic wave modes following Gill (1982). We combine full-depth CTD observations from the *Ronald H. Brown* with glider observations in the upper 1,000 m to produce a composite full-depth profile of Brunt-Väisälä frequency. We do not attempt to account for the effects of mean zonal flows on the baroclinic modes (see McPhaden et al., 1987).

Low-pass-filtered ADT within 1.5° of latitude of the equator (Figure 3b) shows an eastward propagating wave of elevated sea level that originated at the western boundary when the sign of the zonal wind stress changed sign around 10 April (Figure 3a). The wave had an eastward phase speed consistent with the 2.8 m s^{-1} speed of the first baroclinic mode for the observed stratification (Figure 3, dashed black line), suggesting that this is a first-mode baroclinic Kelvin wave. The elevated sea level is consistent with both the relaxation of westward winds leading to release of waters that had been pushed against the western boundary and the depression of near-surface isopycnals observed in successive cross-equator transects (Figure 2). The ADT in Figure 3b likely also includes influence from forced and reflected Rossby waves of various modes as well as reflected Kelvin waves (e.g., Nagura & McPhaden, 2010).

Despite the arrival of a first-mode baroclinic Kelvin wave following the change in zonal winds along the equator, the vertical structure of the observed zonal velocity changes is inconsistent with the first baroclinic mode. Using the weighted least squares technique of Rudnick et al. (2017), we fit a time-mean (Figure 5a) and linear trend (Figure 5b) to the the zonal velocity observations from the five cross-equator transects (Figure 2, left). The mean zonal velocity over March–May 2018 most closely matches the two transects occupied during 4 April to 5 May (Figures 2c and 2e) near the midpoint of the observing period, with lateral

smoothing from the Gaussian weighting used in the fit (Rudnick et al., 2017). Consistent with the discussion in sections 3.1.1 and 3.1.2, the linear trend in zonal velocity (Figure 5b) during March–May 2018 has an eastward acceleration of approximately 0.02 m s^{-1} per day from the surface to about 50 m (except near 1.5°S where it reaches to near 100 m), a westward acceleration of about 0.01 m s^{-1} per day from about 50 to 150 m, and weaker acceleration below that. The meridionally averaged linear trend (Figure 5c, blue) has a zero crossing at 59 m and again approaches 0 near 210 m. The shallowest zero crossing of the computed first baroclinic mode, however, is at 1,477 m. Indeed, the mode with its shallowest estimated zero crossing nearest to 59 m is the sixth baroclinic mode at 62 m. We note also that the second baroclinic mode, which is resonantly forced by semiannual winds in the Indian Ocean (Jensen, 1993; Nagura & McPhaden, 2010), crosses 0 at 208 m (Figure 5, red squares), approximately the depth at which the trend in observed zonal velocity approaches 0.

It appears that a first-mode baroclinic Kelvin wave alone is insufficient to explain the rapid evolution of equatorial circulation during March–May 2018. Contributions from higher vertical modes are needed to produce the shallow sign reversal of the temporal trend in zonal velocity. Though we have neglected the effects of mean zonal currents in our computation of baroclinic modal structure, the analysis by McPhaden et al. (1987) indicates that the effect of including realistic zonal velocities in the normal mode computation can shift zero crossings by O(100) m, far too little to bring the first mode into agreement with the observed vertical structure (Figure 5c). Uncertainty in computed zero crossing depths for successive modes arising from the combination of our neglect of mean flows, the 10-m vertical resolution of the observations, and spatial and temporal variability in stratification precludes precise determination of which higher modes are at play since their shallowest zero crossings are closely spaced (Figure 5c).

The apparent impact of higher-order modes found here is consistent with the numerical results of Chen et al. (2015), who suggested that Modes 3–8 were important contributors to EUC evolution. Likewise, high-vertical-mode Kelvin waves have been shown to be important in the variability of stacked jets at the equator (Eden & Dengler, 2008) and to play a role in fluctuations of equatorial Pacific circulation during El Niño events (Firing et al., 1983). The phase speeds of these higher modes (ranging from about 1.1 m s^{-1} for Mode 3 to about 0.4 m s^{-1} for Mode 8) are too slow for the signal of the winds changing sign at the western boundary to reach the observation region near 57°30′E during the observation period. Though not readily apparent in low-pass-filtered absolute dynamic topography (Figure 3b), perhaps higher-mode waves are generated locally and subsequently impact the vertical structure of the equatorial circulation changes during the monsoon transition. Nagura and McPhaden (2010) demonstrate that sea surface height is more strongly impacted by the first baroclinic mode than is zonal velocity. Alternatively, Eden and Dengler (2008) hypothesize that instabilities in the Somali current, which reverses seasonally (e.g., Schott & McCreary, 2001), may excite high baroclinic modes and thereby contribute the high-mode structure of equatorial currents in the Indian Ocean.

3.2. Supply of High-Salinity Water to the Bay of Bengal by the EUC

When present, the eastward EUC in boreal spring 2018 carried waters with maximum salinity exceeding 36.3 g kg^{-1} (Figures 2b, 2d, and 4c). Found primarily north of the equator at potential densities near 24 kg m^{-3}, these high-salinity waters most likely originated in the evaporative Arabian Sea and have properties consistent with ASHSW. Notably, our observations show evidence of ASHSW much farther south in March–May than did the ship-based observations through 1994 that were available to Kumar and Prasad (1999). As the EUC weakened and vanished, maximum salinities decreased by 0.2–0.5 g kg^{-1}, particularly north of the equator (Figures 2i, 4b, and 4c).

The EUC in late March–early April 2018 was stronger and saltier than during the same period of 2017, when the maximum speed observed by a glider was 0.75 m s^{-1}, maximum salinity was 36.0 g kg^{-1} (Centurioni et al., 2017, their Figure 5), and eastward transport shallower than 180 m and from 1.5°S to 1°N (the northern extent of observations in 2017) was only 10.7 Sv. EUC properties in 2018 are similar to those described by Sanchez-Franks et al. (2019) in numerical simulations for the years 2007, 2014, and 2015 when the EUC was anomalously strong during the spring intermonsoon at 65°E. However, the ENSO state as indicated by the Oceanic Niño Index (3-month running mean of SST anomaly in the Niño 3.4 region) was more strongly positive at the end of the large 2015–2016 El Niño in March–May 2016 (+1.03) than in March–May 2017 (+0.29), contrary to the positive correlation between ENSO and Indian EUC strength a year later found by Sanchez-Franks et al. (2019) for prior years. We note also that both March–May 2017 and March–May 2018

were periods of weakly positive Dipole Mode Index (Saji et al., 1999) (averages of 0.56 and 0.36, respectively), so that the state of the Indian Ocean Dipole seems unlikely to explain the differences in EUC strength and water properties, consistent with the results of Sanchez-Franks et al. (2019).

Glider observations along 85°45′E in the southern Bay of Bengal captured a particularly salty HSC extending to nearly 9°N by late June 2018 (Figure 2k). Salinities greater than 35.2 g kg^{-1} were found in a roughly 30-m-thick layer centered near a depth of 110 m at the southern end of the transect and shoaling to near 70 m in the north. The density of the HSC increased slightly from south to north, being centered on 23.0 kg m^{-3} isopycnal in the south and found between the 23.0 and 24.0 kg m^{-3} isopycnals in the north, indicating cooling of the HSC to the north (Figure 2k). In temperature-salinity space, HSC waters observed in June 2018 were similar to waters found in the western equatorial Indian Ocean in March–May 2018 (Figure 4c). In agreement with the mechanism posited by Sanchez-Franks et al. (2019), it seems likely that the strong EUC in the western Indian Ocean during the spring intermonsoon of 2018 fed the HSC in the Bay of Bengal in summer 2018. Observed O(1) m s^{-1} speeds in the EUC (Figures 2 and 4) were sufficient to have allowed waters to traverse the roughly 3,500 km between survey locations in the western equatorial Indian Ocean and the southern Bay of Bengal during the approximately two months between sampling in the two locations.

4. Summary

A set of five cross-equator transects occupied by an underwater glider and a research vessel in March–May 2018 to the northeast of the Seychelles (Figure 1) provide a detailed view of circulation in the western equatorial Indian Ocean. These new observations capture the oceanic response to the transition from the northeast (boreal winter) monsoon to the southwest (boreal summer) monsoon in an oceanic region that has been very sparsely observed in recent decades. Prior to the monsoon transition, currents were westward at O(1) m s^{-1} near the surface and similarly fast, but oppositely directed, in the EUC from 40–150 m. The EUC carried the saltiest waters observed (Figures 2a, 2b, and 4), which likely originated in the evaporative Arabian Sea. Over the following 1–2 months, near-surface flow reversed as a Wyrtki Jet formed, the EUC vanished, and waters typically freshened modestly (Figures 2c–2j and 4) as the eastward zonal winds set in during the monsoon transition (Figure 3a). The EUC in March–May 2018 was stronger than in the preceding year, providing a pathway for ASHSW from the western equatorial Indian Ocean to feed the subsurface high-salinity core observed in the southern Bay of Bengal in summer 2018 (Figures 2k and 4c) via the mechanism of Sanchez-Franks et al. (2019). Further observing effort is needed in the western equatorial Indian Ocean in order characterize the full annual cycle of the circulation and to constrain interannual variability.

Although a first-mode equatorial Kelvin wave originated at the western boundary and traveled through the observation region during the monsoon transition (Figure 3b), that wave alone could not account for the evolution of equatorial circulation. The profile of zonal acceleration constructed from the repeat transects (Figure 5c) has a zero crossing at a depth of 59 m, much shallower than the zero crossing for the first baroclinic mode and consistent with higher baroclinic modes. Further investigation, likely using realistic numerical simulations constrained by observations, is needed to clarify the role of these higher baroclinic modes during monsoon transitions.

Acknowledgments
Spray glider operations would not have been possible without the support of Patrick Deane, Larry George, and Joleen Heiderich from WHOI and Jeff Sherman, Ben Reineman, and the Instrument Development Group at the Scripps Institution of Oceanography. Support for operations in the Seychelles was provided by the Seychelles Coast Guard, the Better Life Foundation, and NASCar collaborators. Hemantha Wijesekera and MISO-BOB colleagues at the Naval Research Laboratory as well as the crew of R/V *Thomas G. Thompson* enabled glider operations in the Bay of Bengal. NASCar Spray glider observations are available from http://spraydata.ucsd.edu and should be cited using the following https://doi.org/10.21238/S8SPRAY0053 (Todd, 2020). Ship-based data were collected and made publicly available by GO-SHIP (http://www.go-ship.org/) and the national programs that contribute to it; we thank I07N chief scientists Viviane Menezes and Denis Volkov for bringing the GO-SHIP data to our attention. CTD data from the *Ronald H. Brown* are available at http://cchdo.ucsd.edu (ExpoCode 33RO20180423); shipboard ADCP data from the cruise are available from the Joint Archive for Shipboard ADCP (http://ilikai.soest.hawaii.edu/sadcp/index.html) with broadband data under SAC ID 02302. Altimetry products are available from CMEMS (http://marine.copernicus.eu). ERA-Interim reanalysis data are available from ECMWF (https://apps.ecmwf.int/datasets/data/interim-full-daily/). The Oceanic Niño Index is available from the NOAA Climate Prediction Center (https://www.cpc.ncep.noaa.gov/data/indices/oni.ascii.txt). The Dipole Mode Index is available from NOAA (https://stateoftheocean.osmc.noaa.gov/sur/ind/dmi.php). This work was supported by the Office of Naval Research as part of the NASCar DRI under Grant N000141512632 and as part of the MISO-BOB DRI under Grant N000141712968.

References

Centurioni, L., Hormann, V., Talley, L. D., Arzeno, I., Beal, L., Caruso, M., et al. (2017). Northern Arabian Sea Circulation-autonomous research (NASCar): A research initiative based on autonomous sensors. *Oceanography*, *30*(2), 92–103. https://doi.org/10.5670/oceanog.2017.227

Chen, G., Han, W., Li, Y., Wang, D., & McPhaden, M. J. (2015). Seasonal-to-interannual time-scale dynamics of the equatorial undercurrent in the Indian Ocean. *Journal of Physical Oceanography*, *45*, 1532–1553. https://doi.org/10.1175/JPO-D-14-0225.1

Dee, D. P., Uppala, S. M., Simmons, A. J., Berrisford, P., Poli, P., Kobayashi, S., et al. (2011). The ERA-Interim Reanalysis: Configuration and performance of the data assimilation system. *Quarterly Journal of the Royal Meteorological Society*, *137*, 553–597. https://doi.org/10.1002/qj.828

Eden, C., & Dengler, M. (2008). Stacked jets in the deep equatorial Atlantic Ocean. *Journal of Geophysical Research*, *113*, C04003. https://doi.org/10.1029/2007JC004298

Firing, E., Lukas, R., Stadler, J., & Wyrtki, K. (1983). Equatorial undercurrent disappears during 1982–1983 El Niño. *Science*, *222*(4628), 1121–1123. https://doi.org/10.1126/science.222.4628.1121

Gill, A. E. (1982). *Atmosphere-ocean dynamics* (vol. 30). San Diego: Calif: Academic Press.

Huang, K., Han, W., Wang, D., Wang, W., Xie, Q., Chen, J., & Chen, G. (2018). Features of the Equatorial Intermediate Current associated with basin resonance in the Indian Ocean. *Journal of Physical Oceanography*, *48*, 1333–1347. https://doi.org/10.1175/JPO-D-17-0238.1

Iskander, I., Masumoto, Y., & Mizuno, K. (2009). Subsurface equatorial zonal current in the eastern Indian Ocean. *Journal of Geophysical Research*, *114*, C06005. https://doi.org/10.1029/2008JC005188

Iskander, I., & McPhaden, M. J. (2011). Dynamics of wind-forced intraseasonal zonal current variations in the equatorial Indian Ocean. *Journal of Geophysical Research*, *116*, C06019. https://doi.org/10.1029/2010JC006864

Jensen, T. G. (1993). Equatorial variability and resonance in a wind-driven Indian Ocean model. *Journal of Geophysical Research*, *98*(C12), 22,533–22,552. https://doi.org/10.1029/93JC02565

Knauss, J. A., & Taft, B. A. (1963). Measurements of currents along the equator in the Indian Ocean. *Nature*, *198*(4878), 376–377.

Knauss, J. A., & Taft, B. A. (1964). Equatorial undercurrent of the Indian Ocean. *Science*, *143*(3604), 354–356.

Knox, R. A. (1974). Reconnaissance of the Indian Ocean equatorial undercurrent near Addu Atoll. *Deep Sea Research*, *21*, 123–129.

Kumar, S. P., & Prasad, T. G. (1999). Formation and spreading of Arabian Sea high-salinity water mass. *Journal of Geophysical Research*, *104*(C1), 1455–1464. https://doi.org/10.1029/1998JC900022

Lee, C. M., Jinadasa, S. U. P., Anutaliya, A., Centurioni, L. R., Fernando, H. J. S., Hormann, V., et al. (2016). Collaborative observations of boundary currents, water mass variability, and monsoon response in the southern Bay of Bengal. *Oceanography*, *29*(2), 102–111. https://doi.org/10.5670/oceanog.2016.43

Leetmaa, A., & Stommel, H. (1980). Equatorial current observations in the western Indian Ocean in 1975 and 1976. *Journal of Physical Oceanography*, *10*, 258–269.

Luyten, J. R., & Roemmich, D. H. (1982). Equatorial currents at semi-annual period in the Indian Ocean. *Journal of Physical Oceanography*, *12*, 406–413. https://doi.org/10.1175/1520-0485(1982)012h0406:ECASAPi2.0.CO;2

McPhaden, M. J. (1986). The equatorial undercurrent: 100 years of discovery. *Eos, Transactions American Geophysical Union*, *67*(40), 762–765.

McPhaden, M. J., Meyers, G., Ando, K., Masumoto, Y., Murty, V., Ravichandrand, M., et al. (2009). RAMA: The Research Moored Array for African Asian-Australian Monsoon Analysis and Prediction. *Bulletin of the American Meteorological Society*, *90*(4), 459–480. https://doi.org/10.1175/2008BAMS2608.1

McPhaden, M. J., Proehl, J., & Rothstein, L. (1987). On the structure of low frequency equatorial waves. *Journal of Physical Oceanography*, *17*, 1555–1559. https://doi.org/10.1175/1520-0485(1987)017h1555:OTSOLFi2.0.CO;2

Nagura, M., & McPhaden, M. J. (2010). Wyrtki Jet dynamics: Seasonal variability. *Journal of Geophysical Research*, *115*, C07009. https://doi.org/10.1029/2009JC005922

Philander, S. G. H. (1973). Equatorial undercurrent: Measurements and theories. *Reviews of Geophysics and Space Physics*, *11*(3), 513–570.

Rao, R. R., & Sivakumar, R. (2003). Seasonal variability of sea surface salinity and salt budget of the mixed layer of the north Indian Ocean. *Journal of Geophysical Research*, *108*(C1), 3009. https://doi.org/10.1029/2001JC000907

Reppin, J., Schott, F. A., Fischer, J., & Quadfasel, D. R. (1999). Equatorial currents and transports in the upper central Indian Ocean: Annual cycle and interannual variability. *Journal of Geophysical Research*, *104*(C7), 15,495–15,514. https://doi.org/10.1029/1999JC900093

Riser, S. C., Freeland, H. J., Roemmich, D., Wijffels, S., Troisi, A., Belbéoch, M., et al. (2016). Fifteen years of ocean observations with the global Argo array. *Nature Climate Change*, *6*, 145–153. https://doi.org/10.1038/NCLIMATE2872

Rochford, D. (1964). Salinity maxima in the upper 1000 meters of the North Indian Ocean. *Australian Journal of Marine and Freshwater Research*, *15*(1), 1–24. https://doi.org/10.1071/MF9640001

Rudnick, D. L., Davis, R. E., & Sherman, J. T. (2016). Spray underwater glider operations. *Journal of Atmospheric and Oceanic Technology*, *33*(6), 1113–1122. https://doi.org/10.1175/JTECH-D-15-0252.1

Rudnick, D. L., Sherman, J. T., & Wu, A. P. (2018). Depth-average velocity from Spray underwater gliders. *Journal of Atmospheric and Oceanic Technology*, *35*, 1665–1673. https://doi.org/10.1175/JTECH-D-17-0200.1

Rudnick, D. L., Zaba, K. D., Todd, R. E., & Davis, R. E. (2017). A climatology of the California Current System from a network of underwater gliders. *Progress in Oceanography*, *154*, 64–106. https://doi.org/10.1016/j.pocean.2017.03.002

Saji, N. H., Goswami, B. N., Vinayachandran, P. N., & Yamagata, T. (1999). A dipole mode in the tropical Indian Ocean. *Nature*, *401*, 360–363. https://doi.org/10.1038/43854

Sanchez-Franks, A., Webber, B. G. M., King, B. A., Vinayachandran, P. N., Matthews, A. J., Sheehan, P. M. F., et al. (2019). The railroad switch effect of seasonally reversing currents in the Bay of Bengal high-salinity core. *Geophysical Research Letters*, *46*, 6005–6014. https://doi.org/10.1029/2019GL082208

Schott, F. A., & McCreary, J. P. Jr. (2001). The monsoon circulation of the Indian Ocean. *Progress in Oceanography*, *51*, 1–123.

Shenoi, S., Shetye, S., Gouveia, A., & Michael, G. (1993). Salinity extrema in the Arabian Sea. In V. Ittekkot, & R. Nair (Eds.), *Monsoon biogeochemistry* (pp. 37–49). Hamburg: Mitt. Geol.-Paläont: Inst., University Hamburg.

Sherman, J., Davis, R. E., Owens, W. B., & Valdes, J. (2001). The autonomous underwater glider "Spray". *IEEE Journal of Oceanic Engineering*, *26*(4), 437–446. https://doi.org/10.1109/48.972076

Sloyan, B. M., Wanninkhof, R., Kramp, M., Johnson, G. C., Talley, L., Tanhua, T., et al. (2019). The Global Ocean Ship-Based Hydrographic Investigations Program (GO-SHIP): A platform for integrated multidisciplinary ocean science. *Frontiers in Marine Science*, *6*, 445. https://doi.org/10.3389/fmars.2019.00445

Swallow, J. C. (1964). Equatorial undercurrent in the western Indian Ocean. *Nature*, *204*(4957), 436–437.

Todd, R. E. (2020). Spray glider observations in support of NASCar [Dataset]. Scripps Institution of Oceanography, Instrument Development Group. http://doi.org/10.21238/S8SPRAY0053

Todd, R. E., Asher, T. G., Heiderich, J., Bane, J. M., & Luettich, R. A. (2018). Transient response of the Gulf Stream to multiple hurricanes in 2017. *Geophysical Research Letters*, *45*, 10,509–10,519. https://doi.org/10.1029/2018GL079180

Todd, R. E., Rudnick, D. L., Sherman, J. T., Owens, W. B., & George, L. (2017). Absolute velocity estimates from autonomous underwater gliders equipped with Doppler current profilers. *Journal of Atmospheric and Oceanic Technology*, *34*(2), 309–333. https://doi.org/10.1175/JTECH-D-16-0156.1

Wyrtki, K. (1973). An equatorial jet in the Indian Ocean. *Science*, *181*, 262–264.

Yuan, D., & Han, W. (2006). Roles of equatorial waves and western boundary reflection in the seasonal circulation of the equatorial Indian Ocean. *Journal of Physical Oceanography*, *36*, 930–944. https://doi.org/10.1175/JPO2905.1